



Effect of Long-Range Corrections on Intermolecular Interactions and Vibrational Assignments of Ethylene Oxide Dimer. A Combined DFT and SQFF Study

Elida Romano 

Cátedra de Química General, Facultad de Bioquímica, Química y Farmacia, Universidad Nacional de Tucumán, Ayacucho 471, 4000, San Miguel de Tucumán, Tucumán, R. Argentina

Maria E. Manzur 

Cátedra de Química General, Facultad de Bioquímica, Química y Farmacia, Universidad Nacional de Tucumán, Ayacucho 471, 4000, San Miguel de Tucumán, Tucumán, R. Argentina

Maximiliano A. Iramain 

Cátedra de Química General, Facultad de Bioquímica, Química y Farmacia, Universidad Nacional de Tucumán, Ayacucho 471, 4000, San Miguel de Tucumán, Tucumán, R. Argentina

Silvia Antonia Brandán  

Cátedra de Química General, Facultad de Bioquímica, Química y Farmacia, Universidad Nacional de Tucumán, Ayacucho 471, 4000, San Miguel de Tucumán, Tucumán, R. Argentina

Suggested Citation

Romano, E., Manzur, M.E., Iramain, M.A. & Brandán, S.A. (2023). Effect of Long-Range Corrections on Intermolecular Interactions and Vibrational Assignments of Ethylene Oxide Dimer. A Combined DFT and SQFF Study. *European Journal of Theoretical and Applied Sciences*, 1(5), 409-425.
DOI: [10.59324/ejtas.2023.1\(5\).32](https://doi.org/10.59324/ejtas.2023.1(5).32)

Abstract:

Theoretical structural and vibrational study for the ethylene oxide dimer have been performed by using the experimental structure determined by X-ray diffraction, the vibrational spectra and, the functional hybrids B3LYP/6-311++G** and WB97XD/6-311++G** methods. Here, the effects of dispersion on intermolecular interactions and on complete assignments of infrared and Raman spectra of dimer have been performed combining the Pulay's scaled quantum mechanical force field (SQMFF) methodology with those two levels of calculations in order to fit the theoretical wavenumbers values to the experimental ones. Calculations including long-range corrections have revealed similar optimized energy, volume and frequencies to calculated with the

B3LYP/6-31G* method, lower correlations in the geometrical parameters, higher stabilization energy, higher values in the topological parameters and higher scaled force constants than the obtained at B3LYP/6-311++G** level. Natural bond order (NBO) and atoms in molecules theory (AIM) studies with both methods reveal two types of intermolecular interactions (C-O...H and C-O...O) in the ethylene oxide dimer in accordance with the bands observed in the experimental Raman spectrum at low temperatures and with the experimental structure determined at 100 K. The nature of those interactions and their topological properties were studied by using NBO and AIM calculations. The studied properties for the ethylene oxide dimer were analyzed and compared with those obtained for the monomer. Similar assignments of the vibrational modes for dimer were obtained using the three different methods.

Keywords: *Ethylene Oxide Dimer; Vibrational Spectra; Molecular Structure; Force Field; DFT Calculations.*



Introduction

Ethylene oxide, (C_2H_4O) is a compound broadly studied from different point of view and by using diverse spectroscopic methods (Bertie & Othen, 2011; Cant & Armstead, 1975; Bertie & Jacobs, 1978; Mills, 1965; Lowe et al., 1986; Hair, Beswick, & Janda, 1988; Winkler et al., 1999; Frimand, & Jalkanen, 2002; Bégué et al., 2007; Bernstein, & Lynch, 2009; Weiyu et al., 2009; Grabowsky et al., 2009). From a chemical point of view, the ethylene oxide monomer is a synthetic intermediate in the preparation of functional materials with desirable properties in the area of new solid polymer electrolytes which are potentially useful electrolytes to be applied in high-energy batteries (Zhang, & Wang, 2009; Polomska et al., 1999; Ali, Mohamed, & Arof, 1998; Daniel, Desbat, & Lassegues, 1988; Zhang et al., 2006; Zhang, & Wang, 2009; Oparaji, O., Zuo, & Hallinan Jr., 2016). The polymerization of ethylene oxide or of a mono-substituted ethylene leads to polymers in the solid state, such as the polyethylene oxide (PEO), whose physical and mechanical properties are strongly dependent of the structure. Particularly, the hydration process of a PEO tablet is of great pharmaceutical interest. The chains of a polymer in the crystalline state are aligned when the polymer is melted; the chain conformations then become disordered and, as a consequence, change the spectra. For these reasons, in many chemical industries new polymer syntheses are carefully controlled by means of infrared and Raman spectra. The infrared and Raman spectra of this epoxide in gas and liquid phases at room temperature and at low temperatures in the solid state, were published and only the assignments for the oxide as monomer were reported previously (Bertie & Othen, 2011; Cant & Armstead, 1975; Bertie & Jacobs, 1978; Mills, 1965; Lowe et al., 1986; Hair, Beswick, & Janda, 1988). The experimental electron density of ethylene oxide was derived by Grabowsky et al. (2008) from a multipole refinement high-resolution X-ray diffraction data collected at 100 K and complemented by density-functional calculations at experimental and optimized geometry. On the other hand, the technique of

electron momentum spectroscopy was employed to measure orbital momentum distributions for the complete valence electronic structure of ethylene oxide (Weiyu et al., 2009). From this study it is possible to derive ethylene oxide's chemically interesting molecular properties, which are subsequently compared with the results of other workers. In this context, intermolecular interactions, such as the hydrogen bonding, play an important role in the determination of the molecular structure and properties of ethylene oxide (Weiyu et al., 2009; Zhang, & Wang, 2009). At this time, the ethylene oxide as monomer was characterized both structural and vibrationally (Bertie & Othen, 2011; Cant & Armstead, 1975; Bertie & Jacobs, 1978; Mills, 1965), but the effects of dispersion on intermolecular interactions of dimer and on the vibrational assignments are not reported yet. Therefore, the aim of this paper is to report a theoretical study on ethylene oxide dimer by using experimental data existing of its structure and vibrational spectra combined with the Pulay's scaled quantum-mechanical force field (SQMFF) methodology and the Molvib program (Pulay et al., 1983; Rauhut, & Pulay, 1995; Sundius, 2002) in order to carry out complete and reliable vibrational analyses taking into account the B3LYP/6-311++G** and WB97XD/6-311++G** methods (Becke, 1988; Lee, Yang, & Parr, 1988; Chai, & Head-Gordon, 2008). For this purpose, we optimized the dimer geometry by using both levels of calculations. Here, we present a detailed study of the vibrational spectra of the ethylene oxide dimer and propose a complete assignment of the observed bands based on a normal coordinate analysis and scaling factors together with the harmonic force fields (Pulay et al., 1983; Rauhut, & Pulay, 1995; Sundius, 2002). In addition, the spectroscopic behaviour of the ethylene oxide dimer was studied and interpreted on the basis of the molecular structure observed experimentally at 100 K (Grabowsky et al., 2009). This way, the presence of bands in the Raman spectrum in the lower wave numbers region assigned to the vibrational modes of the dimer justifies its presence at low temperature in

the solid phase. In addition, the nature of the two types of intermolecular interactions found in the dimer (C-O \cdots H and C-O \cdots O) were studied by means of the natural bond orbital analysis (NBO) (Glendening et al., 1996) while their topological properties were analyzed using the atoms in molecules theory (AIM) calculations (Bader, 1990; Biegler-Konig, Schonbohm, & Bayles, 2001). Here, the theoretical molecular, vibrational and topological properties of the ethylene oxide dimer are shown and compared with those obtained experimentally for the monomer.

Computational Details

The starting point for the geometry optimization of the ethylene oxide dimer was a structure with the bonds lengths and angles taken from the experimental structure derived by Grabowsky et al. (2008) from a multipole refinement high-resolution X-ray diffraction data collected at 100 K. The initial structure was modelled with the *GaussView* program (Nielsen, & Holder, 2008) and the calculations were made with the functional hybrids B3LYP/6-311++G** and WB97XD/6-311++G** methods (Becke, 1988; Lee, Yang, & Parr, 1988; Chai, & Head-Gordon, 2008) as implemented in the Gaussian 09 set of programs (Frisch et al., 2009). The optimized structures for the monomer (EOM) and dimer (EOD) together with the corresponding numbering of atoms for both forms and the CIF file are shown in **Figure 1**.

The normal internal coordinates for EOD are shown in **Table S1** (Supporting Material), and they were defined as those proposed by Fogarasi et al. (1992). The harmonic force field Cartesian coordinates for the dimer that resulted from the calculations were turned into "natural" internal coordinates by the Molvib program (Sundius, 2002). The Potential Energy Distribution (PED) components larger than or equal to 10% were subsequently calculated with the Scaled Quantum Mechanics (SQM) force field. Furthermore, an NBO analysis was then performed by using the two calculation levels with the NBO 5.0 program (Glendening et al., 1996) included in the Gaussian 03 package (Chai,

& Head-Gordon, 2008). The topological properties of the charge density for the dimer were computed at the same theory levels with the AIM2000 software (Bader, 1990; Biegler-Konig, Schonbohm, & Bayles, 2001). We clarify that the total energy values for EOD were not corrected for the basis set superposition error (BSSE) by the standard Boys–Bernardi counterpoise method because the energy differences with the 6-311++G** basis set are negligible, as was also observed for other dimeric species (Boys, & Bernardi, 1970; Brandán et al., 2010).

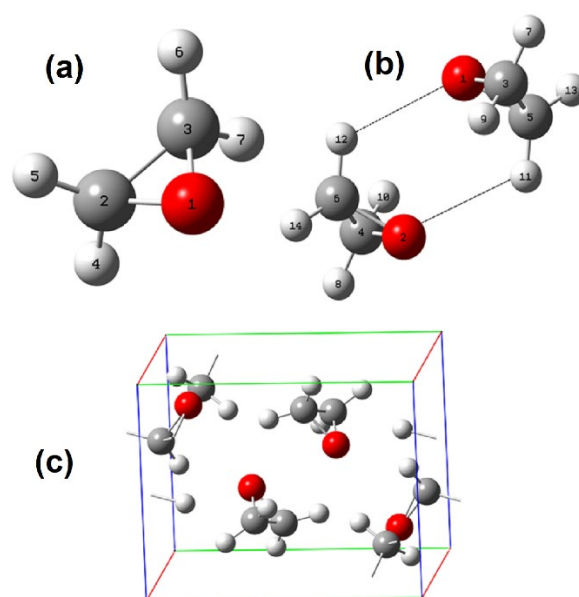


Figure 1. Theoretical Structures and Numbering of Atoms for Ethylene Oxide as: a) Monomer, b) Dimer Showing the Intramolecular H-Bonds with Dashed Lines and c) Crystal Packing of Ethylene Oxide Dimer Determined by X-Ray Diffraction

Source: Grabowsky et al., 2008

Results and Discussion

Geometry

Table 1 shows the calculated total energies, dipole moments and volume for EOD dimer by using both B3LYP/6-311++G** and WB97XD/6-311++G** methods (Becke, 1988;

Lee, Yang, & Parr, 1988; Chai, & Head-Gordon, 2008) compared with the obtained for the monomer by using two methods. The dipole moment is a relevant property to understand the

stability and reactivity of a compound and, therefore, a comparison of the theoretical dipole moment values for EOM and EOD are also observed in Table 1.

Table 1. Calculated Total Energy (E), Dipolar moments (μ) and Volume (V) for Ethylene Oxide Monomer and Dimer at Different Theory Levels

Method	E (Hartrees)	μ (D)	V (\AA^3)
Monomer			
B3LYP/6-31G*	-153.7863	1.95	64.5
B3LYP/6-311++G**	-153.8361	2.11	64.4
Dimer			
B3LYP/6-31G*	-307.5790	0.00	110.1
B3LYP/6-311++G**	-307.6760	0.26	115.6
WB97XD/6-311++G**	-307.5730	0.00	110.0

Note: B3LYP/6-31G*: $2 \times (-153.7863) = -307.5726$ Hartrees; B3LYP/6-311++G**: $2 \times (-153.8361) = -307.6722$ Hartrees

First of all, it is observed that for both forms the highest dipole moment values and the most stable structures are obtained with the B3LYP/6-311++G** method and, the second one, the total energy for the dimer with both basis sets, is smaller than the sum of the energies of each monomer, for instance, by using the 6-31G* basis set the E value -307.5790 Hartrees is more negative than $2 \times (-153.7863) = -307.5726$ Hartrees. This possibly indicates that the presence of the dimer even in gas phase is preferable to the isolated monomer. This result is very important and it will be taken into consideration in the assignment of the vibrational spectra registered for this compound. Thus, to perform the vibrational analysis by using the most stable structure the best method is B3LYP/6-311++G**, as was also observed in other species (Scheuermann et al., 2018; Sundius, & Brandán, 2023). In addition, the B3LYP/6-31G* calculations for monomer and dimer were also presented because the WB97XD/6-311++G** level of theory for the dimer produces an energy value (-307.5730 Hartrees) similar to obtained with the B3LYP/6-31G* method (-307.5790 Hartrees). Moreover, the dipole moment value increases when the 6-311++G** basis set is used. When the volumes are analysed for the different methods, newly is

observed that the B3LYP/6-31G* method predict practically the same V for the dimer than the WB97XD/6-311++G** level of theory.

The total energy values for the dimer uncorrected while corrected for BSSE effects using the counterpoise method with the B3LYP/6-31G* method are respectively -307.5790 and -307.5751 Hartrees (Boys, & Bernardi, 1970). The BSSE value for the dimer is negligible with the larger basis set (6-311++G**), as was also observed for the dimer of 4-hydroxybenzoic acid (Brandán et al., 2020).

Geometrical parameters

Table 2 shows a comparison of the optimized geometrical parameters for EOD calculated by using the B3LYP and WB97XD methods with the corresponding experimental values which were obtained by Grabowsky et al. (2008) from a multipole refinement by X-ray diffraction data collected at 100 K and complemented by density-functional calculations at experimental and optimized geometry, as shown in Figure 1c. A comparison of all the calculated geometrical parameters with the available experimental data in terms of root-mean-square deviation (RMSD) demonstrates a very good concordance among them. Thus, analysing the bond lengths and

angles it is observed that the B3LYP method generate the lower values (0.025 Å and 0.7°) than the other one (0.096 Å and 0.8°). In the same way, the predicted dihedral angles with the WB97XD method are slightly higher than the

theoretical obtained with the other method. Hence, clearly it is observed that better results are obtained with the B3LYP/6-311++G** method.

Table 2. Comparison of Calculated Geometrical Parameters for Ethylene Oxide Monomer and Dimer with the Corresponding Experimental Values

Parameter	B3LYP/6-311++G**	WB97XD/6-311++G**	Exp ^b 100 K X-ray
	Dimer ^a	Dimer ^a	
Bond lengths (Å)			
C3-H7	1.086	1.086	1.098
C3-H9	1.085	1.086	1.098
C4-H8	1.086	1.086	1.098
C4-H10	1.085	1.086	1.098
C5-H11	1.085	1.086	1.098
C5-H13	1.086	1.086	1.099
C6-H12	1.085	1.086	1.098
C6-H14	1.086	1.086	1.099
C3-C5	1.465	1.461	1.456
C4-C6	1.465	1.461	1.456
C3-O1	1.435	1.422	1.433
C5-O1	1.435	1.422	1.441
C4-O2	1.435	1.422	1.433
C6-O2	1.435	1.422	1.441
O1-H12	2.809	2.609	2.811
O1-H10	2.786	2.647	2.791
O2-H11	2.809	2.609	2.811
O2-H9	2.786	2.647	2.791
O1-O2	3.255	3.134	3.355
RMSD	0.025	0.096	
Bond angles (°)			
H7-C3-H9	116.4	116.6	116.5
H8-C4-H10	116.4	116.6	116.5
H11-C5-H13	116.3	116.7	116.2
H12-C6-H14	116.3	116.7	116.2
C3-O1-C5	61.4	61.8	60.8
C4-O2-C6	61.4	61.8	60.8
O1-C3-C5	59.2	59.1	59.8
O2-C4-C6	59.2	59.1	59.8
H7-C3-O1	114.8	114.9	113.8
H9-C3-O1	114.7	114.8	115.9
H8-C4-O2	114.8	114.9	113.8
H10-C4-O2	114.7	114.8	115.9
RMSD	0.7	0.8	

Dihedral angles (°)			
H7-C3-C5-H11	153.6	153.6	154.7
H7-C3-C5-H13	0.0	-0.0	0.0
H8-C4-C6-H12	-153.6	-153.6	-154.7
H8-C4-C6-H14	-0.0	0.0	-0.0
H7-C3-O1-C5	111.1	110.9	111.2
H11-C5-O1-C3	109.8	109.4	112.1
H8-C4-O2-C6	-111.1	-110.9	-111.2
H12-C6-O2-C4	-109.8	-109.4	-112.1
RMSD	1.3	1.5	

Note: ^aThis work, ^b Source: Grabowsky et al., 2008

Then, if the dispersion by using the WB97XD method is considered the energy value is lower and, besides, the predicted structure at this level of calculations shows lower concordances in the geometrical parameters with the corresponding experimental one than the B3LYP/6-311++G** method. In this context, the vibrational analysis and assignments of infrared and Raman spectra for the dimer must be performed with the better method, which is B3LYP/6-311++G**.

Atomic Charges, Molecular Electrostatic Potentials and Bond Orders

Atomic charges, molecular electrostatic potentials and bond orders are interesting parameters to investigate the characteristics of different bonds and those sites or regions where the reactions with different reactive take places. Thus, for the dimer the Merz-Kollman (MK), Mulliken and natural atomic population (NPA) were computed with both methods (Glendening

et al., 1996; Besler, Merz, & Kollman, 1990). In Table 3 are shown these three types of charges while Figure 2 shows its different behaviours. The detailed analysis of three charges from Fig. 2 show that with both methods the MK (blue colour) and NPA (grey colour) follow approximately a same tendency while the Mulliken charges (orange colour) calculated with the B3LYP method evidence practically the same values on the O and C atoms but with the other method they are different. Thus, with the WB97XD method the MK and Mulliken charges computed show higher differences on the O and C atoms while the three charges on H13 and H14 present the same values with this method, as observed in Table 3. On the other side, the NPA charges predict with both methods the most negative values on O atoms while the most positive on those H9, H10, H11 and H12 atoms because these atoms are involved in the formation of H bonds, as was experimentally observed (Grabowsky et al., 2008).

Table 3. Atomic Charges[#] (MK, Mulliken, NPA) for Ethylene Oxide Dimer at Different Levels of Theory

Atoms	6-311++G** Basis set					
	B3LYP			WB97XD		
	MK	Mulliken	NPA	MK	Mulliken	NPA
1 O	-0.253	-0.185	-0.562	-0.249	-0.156	-0.563
2 O	-0.250	-0.185	-0.562	-0.246	-0.156	-0.563
3 C	-0.173	-0.207	-0.076	-0.180	-0.257	-0.080
4 C	-0.164	-0.207	-0.076	-0.172	-0.257	-0.080
5 C	-0.206	-0.209	-0.076	-0.237	-0.252	-0.080
6 C	-0.212	-0.209	-0.076	-0.243	-0.252	-0.080
7 H	0.152	0.151	0.172	0.158	0.175	0.174
8 H	0.149	0.151	0.172	0.155	0.175	0.174

9 H	0.155	0.150	0.185	0.161	0.157	0.187
10 H	0.153	0.150	0.185	0.158	0.157	0.187
11 H	0.163	0.149	0.185	0.172	0.157	0.188
12 H	0.166	0.149	0.185	0.175	0.157	0.188
13 H	0.161	0.151	0.172	0.174	0.175	0.174
14 H	0.160	0.151	0.172	0.174	0.175	0.174

Note: #Atomic units

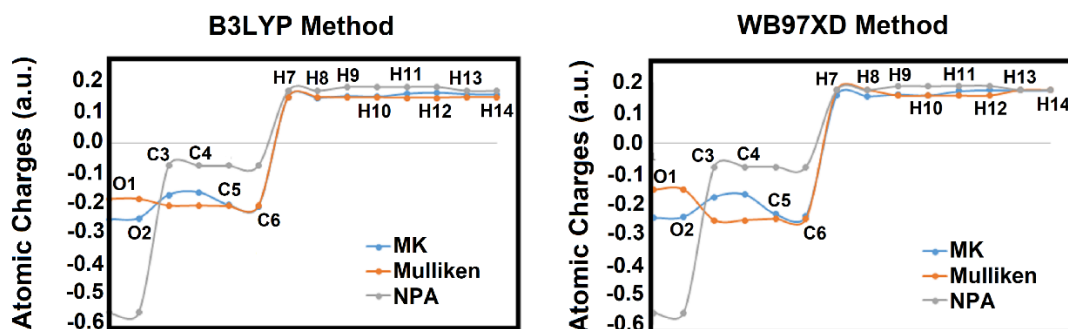


Figure 2. Behaviours of Atomic Charges (MK, Mulliken, NPA) for Ethylene Oxide Dimer at Different Levels of Theory

Regarding the molecular electrostatic potentials (MEP) from Table 4 it is observed similar values for both methods although the B3LYP method shows the higher values on O atoms but lower on the C ones. However, both methods evidence the same values on the H atoms.

If now the mapped MEP surfaces are graphed for the two methods in order to see the different electrophilic and nucleophilic regions, these are those regions with blue and red colours, respectively which represent acceptors and donor's sites of H bonds.

In Figure 3 are observed the different colorations obtained for both methods. Here, on the O atoms of both graphics of Fig. 3 are observed red colours indicating the presences of lone pairs which are acceptors of H bonds while on the H7, H8, H13 and H14 atoms are observed light blue colours indicating the most labile atoms whose MEP values show less negative values with both methods (Table 4).

Then, the green colours represent inert sites where the reactions are not performed.

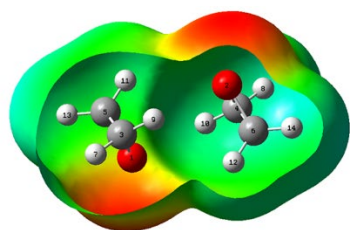
The analysis of the bond orders totals by atoms, expressed by Wiberg's indexes, for EOD (Table

4) shows similar values for all atoms with both methods indicating that the dispersion has not effect on the bond orders. However, the Wiberg bond index matrix in the NAO basis show eight interactions, four of them between the O1 with the H7, H9, H11, H13 atoms and other four between the O2 with the H8, H10, H12, H14 atoms. The bond orders values of those interactions are between 0.0222 and 0.0223.

Table 4. Molecular Electrostatic Potentials and Bond Orders, Expressed as Wiberg Indexes for Ethylene Oxide Dimer at Different Levels of Theory

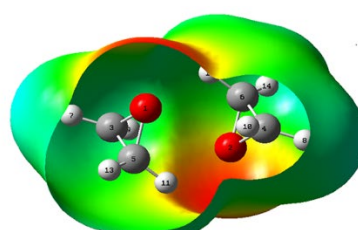
6-31++G** Basis set				
Atoms	B3LYP		WB97XD	
	MEP (a.u.)	BO	MEP (a.u.)	BO
1 O	-22.363	1.939	-22.359	1.938
2 O	-22.363	1.939	-22.359	1.938
3 C	-14.723	3.826	-14.724	3.824
4 C	-14.723	3.826	-14.724	3.824
5 C	-14.723	3.826	-14.725	3.824
6 C	-14.723	3.826	-14.725	3.824
7 H	-1.105	0.973	-1.106	0.972
8 H	-1.105	0.973	-1.106	0.972
9 H	-1.109	0.970	-1.109	0.968

10 H	-1.109	0.970	-1.109	0.968
11 H	-1.109	0.970	-1.109	0.968
12 H	-1.109	0.970	-1.109	0.968
13 H	-1.105	0.973	-1.106	0.972



B3LYP/6-311++G**
±0.0413 a.u.

14 H	-1.105	0.973	-1.106	0.972
------	--------	-------	--------	-------



WB97XD/6-311++G**
±0.0415 a.u.

Figure 3. Calculated Electrostatic Potential Surfaces on the Molecular Surfaces of Ethylene Oxide Dimer in Gas Phase at Different Levels of Theory. Isodensity Value of 0.005

NBO and AIM Studies

The stability of the EOD structures for both levels of theory were also investigated by means of NBO and AIM calculations (Glendening et al., 1996; Bader, 1990; Biegler-Konig, Schonbohm, & Bayles, 2001). The second order perturbation energies $E^{(2)}$ (donor \rightarrow acceptor) that involve the most important delocalization are summarized in Table 5.

Table 5. Main Delocalization Energy (in kJ/mol) for Ethylene Oxide Dimer at Different Levels of Theory

Delocalization	6-311++G**	
	B3LYP	WB97XD
σ O1-C3 \rightarrow σ^* O1-C5	22.4	27.3
σ O1-C3 \rightarrow σ^* C3-C5	11.1	13.5
σ O1-C5 \rightarrow σ^* O1-C3	22.4	27.3
σ O1-C5 \rightarrow σ^* C3-C5	11.1	13.5
σ O2-C4 \rightarrow σ^* O2-C6	22.4	27.3
σ O2-C4 \rightarrow σ^* C4-C6	11.1	13.5
σ O2-C6 \rightarrow σ^* O2-C4	22.4	27.3
σ O2-C6 \rightarrow σ^* C4-C6	11.1	13.5
$\Delta E_{T\sigma \rightarrow \sigma^*}$	134	163.2
LPO1 \rightarrow σ^* C3-H7	20.7	27.7
LPO1 \rightarrow σ^* C3-H9	22.1	29.4
LPO1 \rightarrow σ^* C5-H11	22.2	29.1
LPO1 \rightarrow σ^* C5-H1)	20.7	27.6
LPO2 \rightarrow σ^* C4-H8	20.7	27.7

LPO2 \rightarrow σ^* C4-H10	22.1	29.4
LP O2 \rightarrow σ^* C6-H12	22.2	29.1
LO2 \rightarrow σ^* C6-H1)	20.7	27.6
$\Delta E_{TLP \rightarrow \sigma^*}$	171.4	227.6
ΔE_{Total}	305.4	390.8

Note: Total energy in bold letter.

For these structures, the contribution of the stabilization energies, due mainly to the $\Delta E_{T\sigma \rightarrow \sigma^*}$ charge transfer, are higher than the other ones $\Delta E_{TLP \rightarrow \sigma^*}$ delocalizations, being majors the values predicted for the WB97XD method. Thus, the total energy values clearly show that the dispersion has effect on stabilization energies of dimer and, that this total energy is higher for the WB97XD level of theory.

The EOD structure was also analysed by means of Bader's electron density topology analysis (Bader, 1990; Biegler-Konig, Schonbohm, & Bayles, 2001). The localization of the Bond Critical Point (BCP) in the electron density, $\rho(r)$ and the Laplacian values, $\nabla^2 \rho(r)$ at these points are important for characterization of the molecular electronic structure in terms of interaction magnitude and nature. The BCP has the typical properties of the closed-shell interaction. That is, the value of $\rho(r)$ is relatively low, the relationship $|\lambda_1|/\lambda_3$ is <1 and $\nabla^2 \rho(r)$ is positive indicating that the interaction is dominated by the charge contraction away from

the interatomic surface toward each nucleus. The charge density and $\nabla^2\rho(r)$ for the calculated BCPs from the topological property analysis for

the dimeric structure are shown in **Table 6** while **Figure 4** shows five new interactions formed.

Table 6. An Analysis of the Ring Critical Points (RCP) for Ethylene Oxide Dimer

Parameter (a.u.)	B3LYP/6-311++G**Method				
	O1...H10	O1...H12	O1...O2	O2...H9	O2...H11
$\rho(r)$	0.0057	0.0054	0.0053	0.0057	0.0054
$\nabla^2\rho(r)$	0.0204	0.0197	0.0203	0.0204	0.0197
$ \lambda_1 /\lambda_3$	0.1573	0.1533	0.1158	0.1573	0.1533
Distance (Å)	2.786	2.809	3.256	2.786	2.809
Parameter	WB97XD/6-311++G**Method				
	O1...H10	O1...H12	O1...O2	O2...H9	O2...H11
$\rho(r)$	0.0076	0.0081	0.0068	0.0076	0.0081
$\nabla^2\rho(r)$	0.0272	0.0286	0,0266	0.0272	0,0286
$ \lambda_1 /\lambda_3$	0.1614	0.1672	0.1040	0.1612	0.1670
Distance (Å)	2.647	2.609	3.134	2.647	2.609

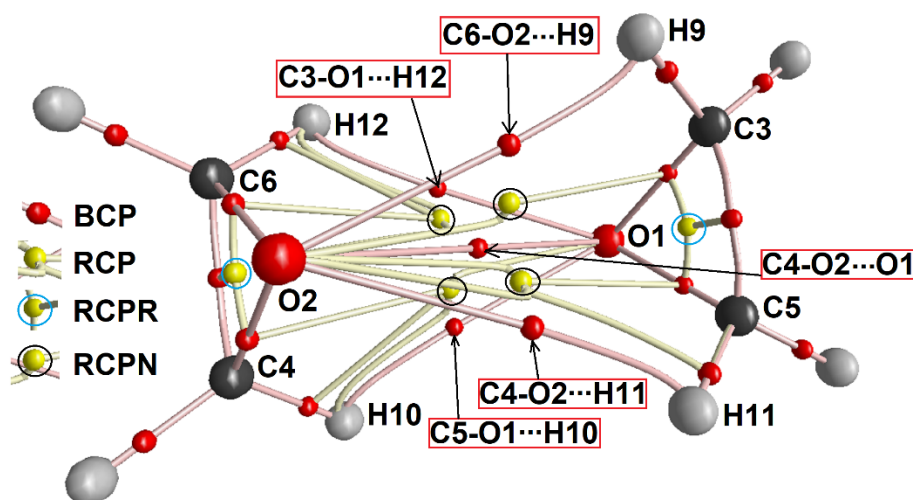


Figure 4. The Five Critical Points of the Charge Density for Ethylene Oxide Dimer Included the O---O Interaction

RCPR correspond to the RCP of two three member's rings (circle blue) while RCPN are the four RCP new. The analysis clearly shows, with both methods, the different nature of those five BCPs, of which four are C3-O1...H12, C4-O2...H11, C5-O1...H10 and C6-O2...H9 interactions and the remaining one is an C4-O2...O1 interaction, as can be seen in Figure 4. These results are in agreement with the NBO

analysis and with the strong intermolecular O-H...O bonds observed experimentally in the solid state at 100 K (Grabowsky et al., 2008). The longer O...O distances (3.256/3.134 Å), as observed in Table 6, probably justify that this BCP can be not experimentally observed. This study evidence higher topological properties and lower distances for the dimer calculated with the WB97XD method.

Vibrational analysis

The infrared spectrum of ethylene oxide in the gas phase was taken from a previous study (Shimanouchi, 1972; NIST, n.a.), which is presented in Figure 5 compared with the corresponding predicted for both methods while the predicted Raman spectra at low temperatures

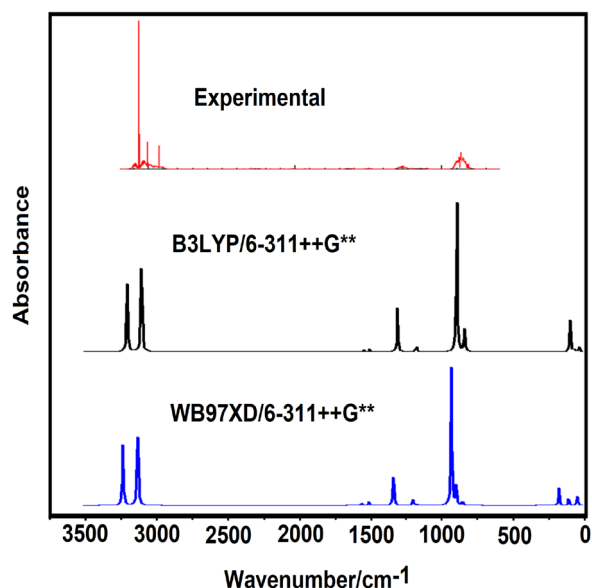


Figure 5. Comparison between Experimental Infrared Spectrum of Ethylene Oxide with the Corresponding Predicted by Using B3LYP/6-311++G and WB97XD/6-311++G** Levels of Theory**

Source: NIST, n.a.

B3LYP/6-31G* and 6-311++G** levels of calculations together with the WB97XD/6-311++G** method have optimized the EOD structure with C_{2h} symmetry and it present 36 normal vibration modes, classified as $18 A_g + 18 A_u$ of which the A_u and A_g modes are active in the infrared and Raman spectra, respectively. The B3LYP/6-31G* level of calculations was also included because the energy obtained at this level is approximately similar to WB97XD

between 140 and 40 cm^{-1} were taken from Bertie & Jacobs (1978) and they are presented in Figures 6 and 7. Here, the predicted infrared spectrum in the lower wavenumbers region ($200\text{-}20 \text{ cm}^{-1}$) can be seen in Figure 6 compared with the corresponding experimental Raman spectra between 140 and 40 cm^{-1} (Bertie & Jacobs, 1978).

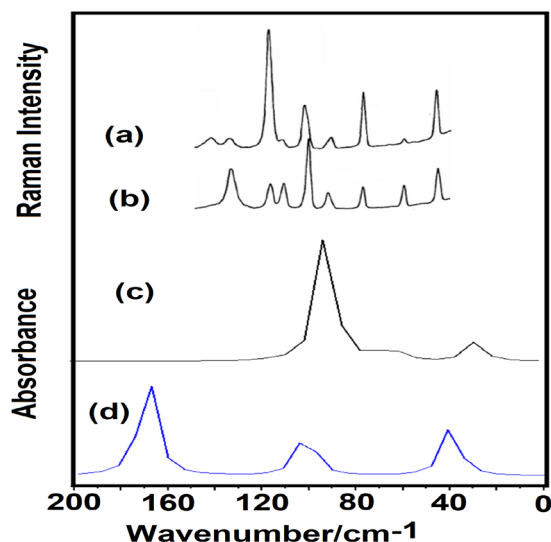


Figure 6. Comparison between: a) Low-Frequency Raman Spectra of Oriented Crystals of Ethylene Oxide at 22 K, Using No Analyzer and Either a Polarization Rotator in the Laser Beam (x(y, x+z)y) or b) not (x(z, x+z)y). c) Predicted Infrared Spectrum of the Ethylene Oxide Dimer at B3LYP and, d) WB97XD/6-311++G Level of Theory in $200\text{-}20 \text{ cm}^{-1}$ Region**

Source: Bertie & Jacobs, 1978

method. The experimental and calculated wavenumbers for the expected normal vibration modes of EOD by using the different levels of theory together with the corresponding assignments are shown in Table 7. Here, the assignments were not separate by the symmetry because these changes for some modes, as observed from the table 7.

Table 7. Observed and Calculated Wavenumbers (cm⁻¹) and Assignment for Ethylene Oxide Dimer by Using Different Levels of Theory

Exp ^b		B3lyp/6-311++G**			B3lyp/6-31G*			Wb97XD/6-311++G**		
IR	Ra	SQM ^c	Assignment ^a	Sym	SQM ^d	Assignment ^a	Sym	SQM ^e	Assignment ^a	Sym
3079		3059	va(CH ₂)o.p	Ag	3083	va(CH ₂)o.p	Ag	3089	va(CH ₂)o.p	Ag
3079		3058	va(CH ₂)i.p	Au	3082	va(CH ₂)i.p	Au	3088	va(CH ₂)i.p	Au
3058	3063w,dp	3045	va(CH ₂)i.p	Ag	3069	va(CH ₂)o.p	Au	3074	va(CH ₂)o.p	Ag
3058		3044	va(CH ₂)o.p	Au	3069	va(CH ₂)i.p	Ag	3074	va(CH ₂)i.p	Au
3019	3005s,p	2966	vs(CH ₂)o.p	Ag	2991	vs(CH ₂)i.p	Au	2993	vs(CH ₂)i.p	Ag
2982		2966	vs(CH ₂)i.p	Au	2991	vs(CH ₂)o.p	Ag	2992	vs(CH ₂)o.p	Au
2945	2961	2960	vs(CH ₂)o.p	Au	2984	vs(CH ₂)o.p	Au	2984	vs(CH ₂)o.p	Au
2913	2916	2960	vs(CH ₂)o.p	Ag	2984	vs(CH ₂)o.p	Ag	2984	vs(CH ₂)o.p	Ag
1500		1469	δ(CH ₂)o.p	Au	1501	δ(CH ₂)o.p	Au	1487	δ(CH ₂)o.p	Au
1487	1490w,p	1458	δ(CH ₂)i.p	Ag	1488	δ(CH ₂)i.p	Ag	1474	δ(CH ₂)i.p	Ag
1470		1431	δ(CH ₂)o.p	Au	1457	δ(CH ₂)o.p	Au	1438	δ(CH ₂)o.p	Au
1451		1428	δ(CH ₂)o.p	Ag	1452	δ(CH ₂)o.p	Ag	1433	δ(CH ₂)o.p	Ag
1273		1259	vs(C-C)	Ag	1272	vs(C-C)	Ag	1287	vs(C-C)	Ag
1270	1266s,p	1258	va(C-C)	Au	1271	va(C-C)	Au	1285	va(C-C)	Au
1168		1142	wag(CH ₂)o.p	Au	1142	wag(CH ₂)o.p	Au	1163	wag(CH ₂)o.p	Ag
1153	1150w,dp	1138	wag(CH ₂)o.p	Ag	1140	wag(CH ₂)o.p	Ag	1158	wag(CH ₂)o.p	Au
1143		1120	wag(CH ₂)i.p	Ag	1140	wag(CH ₂)i.p	Ag	1148	wag(CH ₂)i.p	Au
1134	1120m,p	1113	wag(CH ₂)i.p	Au	1132	wag(CH ₂)i.p	Au	1137	wag(CH ₂)i.p	Ag
1092		1101	ρ(CH ₂)i.p	Au	1112	ρ(CH ₂)i.p	Ag	1124	ρ(CH ₂)i.p	Au
1092		1099	ρ(CH ₂)o.p	Ag	1106	ρ(CH ₂)o.p	Au	1120	ρ(CH ₂)o.p	Ag
		1050	τ _w (CH ₂)o.p	Ag	1065	τ _w (CH ₂)o.p	Au	1057	τ _w (CH ₂)i.p	Ag
		1049	τ _w (CH ₂)i.p	Au	1065	τ _w (CH ₂)i.p	Ag	1056	τ _w (CH ₂)o.p	Au
		989	ρ(CH ₂)o.p	Au	995	ρ(CH ₂)o.p	Au	1012	ρ(CH ₂)o.p	Au
		986	ρ(CH ₂)o.p	Ag	991	ρ(CH ₂)o.p	Ag	1006	ρ(CH ₂)o.p	Ag
897	867m,dp	851	va(C-O)o.p	Au	868	va(C-O)o.p	Au	886	va(C-O)o.p	Au
892		846	vs(C-O)i.p	Ag	864	vs(C-O)i.p	Ag	881	vs(C-O)i.p	Ag
882		799	vs(C-O)o.p	Ag	817	vs(C-O)o.p	Ag	853	vs(C-O)o.p	Ag
821	815	798	va(C-O)i.p	Au	816	va(C-O)i.p	Au	852	va(C-O)i.p	Au
800	807m,dp	737	τ _w (CH ₂)o.p	Ag	742	τ _w (CH ₂)o.p	Au	752	τ _w (CH ₂)o.p	Ag
		736	τ _w (CH ₂)i.p	Au	742	τ _w (CH ₂)i.p	Ag	751	τ _w (CH ₂)i.p	Au
		111	τ(O---H)	Ag	116	δ(O---H)	Ag	164	δ(O---H)	Ag
	101#	84	va(O---H)	Au	115	va(O---H)	Au	162	va(O---H)	Au
	96#	69	δ(O---H), vs(O---H)	Ag	90	vs(O---H)	Ag	134	vs(O---H)	Ag

	71#	58	$\gamma(\text{O---H})_{\text{o.p}}$	Au	76	$\gamma(\text{O---H})_{\text{o.p}}$	Au	91	$\gamma(\text{O---H})_{\text{o.p}}$	Au
	44#	25	$\gamma(\text{O---H})_{\text{i.p}}$	Au	50	$\tau(\text{O---H})$	Ag	37	$\tau(\text{O---H})$	Ag
	44#			Ag	42	$\gamma(\text{O---H})_{\text{i.p}}$	Au	36	$\gamma(\text{O---H})_{\text{i.p}}$	Au

Note: Abbreviations: ν , stretching; δ , deformation; γ , deformation out of plane; wag, wagging; τ , torsion; ρ , rocking; τw , twisting; a, antisymmetric; s, symmetric; s, strong; m, medium; w, weak; p, polarized; dp, depolarized; op, out-of-phase; ip, in-phase. ^aThis work, ^bFrom Winkler et al., 1999, ^cFrom scaled quantum mechanics force field at B3LYP/6-311++G**, ^dFrom scaled quantum mechanics force field at B3LYP/6-31G*, ^eFrom scaled quantum mechanics force field at WB97XD/6-311++G**. Sym, symmetries of vibration modes.

An agreement between theoretical and available experimental results is found, especially in the lower wavenumbers region, as seen in Figure 6. It is important to mention that in the theoretical IR spectrum of monomer there are not observed bands in the vibrational spectra from 500 to 10 cm^{-1} , while in the infrared spectrum of the dimer the vibration normal modes corresponding to the dimeric species are evidenced in that region.

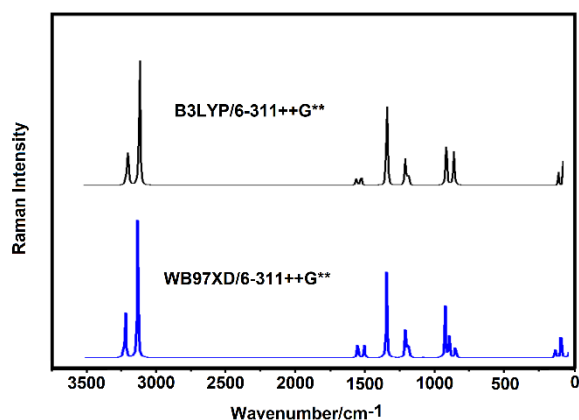


Figure 7. Comparison between Predicted Raman Spectra of Ethylene Oxide by Using the B3LYP/6-311++G and WB97XD/6-311++G** Levels of Theory**

The vibrational assignment of the experimental bands to the normal vibration modes is based on the comparison with related molecules (Bertie & Othen, 2011; Cant & Armstead, 1975; Bertie & Jacobs, 1978; Mills, 1965; Lowe et al., 1986; Hair, Beswick, & Janda, 1988; Winkler et al., 1999; Frimand, & Jalkanen, 2002; Bégué et al., 2007; Bernstein, & Lynch, 2009; Shimanouchi, 1972)

and with the results of the calculations carried out in this investigation. It is important to note that some modes with A_g or A_u symmetries are observed in the IR and Raman spectra probably because the involved modes are not totally antisymmetric or symmetric. The wavenumbers, infrared and Raman intensities and potential energy distribution obtained for EOD by using the B3LYP/6-31G* method is shown in Table S2. The SQM force fields for EOD can be obtained at request. The discussion of the assignments of the most important groups is presented as follows.

Assignments

CH₂ modes

The 3080–2800 cm^{-1} region is characteristic of the CH₂ stretching modes (Bertie & Othen, 2011; Cant & Armstead, 1975; Bertie & Jacobs, 1978; Mills, 1965; Lowe et al., 1986; Hair, Beswick, & Janda, 1988; Winkler et al., 1999; Frimand, & Jalkanen, 2002; Bégué et al., 2007; Bernstein, & Lynch, 2009; Brandán, 2021; Iramain et al., 2022; Issaoui et al., 2017; Mortada et al., 2022), for this, the bands in both spectra between 3079 and 3044 cm^{-1} are assigned to the antisymmetric stretching modes while the corresponding symmetric modes bands are associated with the IR and Raman bands located between 3019 and 2913 cm^{-1} . Here, as predicted by the calculation, the four expected CH₂ bending modes for the dimer are associated with the observed bands in both spectra between 1500 and 1451 cm^{-1} while the wagging modes were predicted between 1163 and 1113 cm^{-1} and, for this reason, they are easily assigned to the IR bands between 1168 and 1134 cm^{-1} . Here, only

rocking and twisting modes were assigned to the IR bands respectively at 1092 and 800 cm^{-1} , as indicated in Table 7.

Skeletal modes

In the dimer, the description of the skeletal stretching modes appears slightly mixed as can be seen in Table S1. The IR bands at 1273 and 1270 cm^{-1} are mainly associated with the C-C stretching modes (Bertie & Othen, 2011; Cant & Armstead, 1975; Bertie & Jacobs, 1978; Mills, 1965; Lowe et al., 1986; Hair, Beswick, & Janda, 1988; Winkler et al., 1999; Frimand, & Jalkanen, 2002; Bégué et al., 2007; Bernstein, & Lynch, 2009; Brandán, 2021; Iramain et al., 2022; Issaoui et al., 2017; Mortada et al., 2022) and the bands between 897 and 821 cm^{-1} , are associated to the C-O stretching modes.

Intermonomer modes

The inter-monomers vibrational modes of the dimer usually observed in the lower wavenumbers region (Brandán et al., 2010; Mortada et al., 2022) and they are related to restricted translations or rotations of one molecule against the other (Table S2). In the 4-hydroxi benzoic acid these six vibration modes

are predicted by B3LYP/6-311++G** calculations between 106 and 18 cm^{-1} (Brandán et al., 2010). Here, the six inter-monomer modes are predicted slightly coupled and they are observed in the Raman spectrum; for this reason, they are assigned as indicated in Table 7. The SQM B3LYP/6-311++G** calculations have no predicted the expected vibration mode at 15 cm^{-1} , and, for this reason, with the aid of *GaussView* that mode was also assigned to torsion dimer mode (Nielsen, & Holder, 2008). Here, clearly the presence of the dimer in the solid state at 100 k justifies the observed bands in the Raman spectra at low temperatures, as reported by Bertie & Jacobs (1978).

Force field

The force constants calculated at B3LYP/6-31G*, B3LYP/6-311++G** and WB97XD/6-311++G** levels of theory EOD were estimated by using the above mentioned scaling procedure by Pulay et al. (1983) and they can be seen in Table 8. The force constants expressed in terms of simple valence internal coordinates were calculated from the corresponding scaled force field by using the Molvib program (Sundius, 2002).

Table 8. Comparison of Scaled Internal Force Constants for Ethylene Oxide Monomer and Dimer

Force constant	Dimer ^a			Monomer	Dimer
	B3LYP		WB97XD		
	6-31G*	6-311++G**	6-311++G**	Mills, 1965	Bichara et al., 2011
$f(\nu\text{C-H})$	5.00	5.08	5.09	4.37	4.89
$f(\nu\text{C-O})$	4.00	3.83	4.29	2.52	6.07
$f(\nu\text{C-C})$	5.40	5.24	5.51	3.57	3.92
$f(\nu\text{O}---\text{H})$	0.03	0.02	0.07		
$f(\delta\text{O}---\text{H})$	0.20	0.16	0.31		

Note: Units are $\text{mdyn } \text{Å}^{-1}$ for stretching and stretching/stretching interactions and $\text{mdyn } \text{Årad}^2$ for angle deformations. ^aThis work, ^bFrom Bichara et al., 2011.

The calculated $f(\nu\text{C-H})$, $f(\nu\text{C-C})$, $f(\nu\text{C-O})$ and $f(\delta(\text{CH}_2))$ force constants values were compared with those obtained by Mills (1965) for the

monomer and with those obtained by Bichara et al (2011) for the citric acid dimer. In general, for EOD an increase in the size of the basis set

diminishes the force constants values while higher values than the other ones are predicted using the WB97XD method. The different calculations procedure probably justifies the observed variations in the force constants. In this case, the values were obtained by means of the SQM procedure while Nakanaga's values were obtained by the iteration method in which the set force constants of Hirokawa were used as the starting values (Mills, 1965). Also, the lower $f(\nu_{C-C})$ and $f(\nu_{C-O})$ force constants values of EOD, in reference to EOM, are attributed to the different interactions that present the former, while the cyclic structure in the ethylene oxide dimer justifies the variations in its force constants in relation to the force constants of the citric acid dimer.

Conclusions

In this work, theoretical molecular structures for the ethylene oxide dimer were determined by using the B3LYP and WB97XD methods and the 6-31G* and 6-311++G** basis sets. Calculations including long-range corrections by using the WB97XD/6-311++G** calculations have revealed that: (i) optimized energy, molecular volume and frequencies are similar to calculated with the B3LYP/6-31G* method, (ii) lower correlations in the geometrical parameters, (iv) higher stabilization energy, (v) higher values in the topological parameters and, (vi) higher scaled force constants than predicted for the B3LYP/6-31G* and B3LYP/6-311++G** methods. NBO and AIM studies with both methods predict five different types of interactions in the ethylene oxide dimer, four of type C-O...H and one C-O...O interaction. Such interactions are assigned to inter-monomers interactions predicted at lower wavenumbers, in accordance with the bands observed in the experimental Raman spectrum at low temperatures and with the experimental structure determined at 100 K. Hence, the presence of bands associated with that stable dimeric structure was detected in the IR and Raman spectra, and complete assignments of the vibrational modes for dimer was accomplished.

Acknowledgements

This work was supported by Consejo de Investigaciones Universidad Nacional de Tucumán (CIUNT) Project No. 26/D714. The authors thank Prof. Sundius for his permission to use MOLVIB.

References

- Ali, A.M.M., Mohamed, N.S., & Arof, A.K. (1998). Polyethylene oxide (PEO)-ammonium sulfate $((NH_4)_2SO_4)$ complexes and electrochemical cell performance. *Journal of Power Sources*, *74*, 135-141.
- Bader, R.F.W. (1990). *Atoms in molecules, a quantum theory*. Oxford: Oxford University Press.
- Becke A. D. (1988). Density-functional exchange-energy approximation with correct asymptotic behavior. *Physical review. A, General physics*, *38*(6), 3098-3100. <https://doi.org/10.1103/physreva.38.3098>
- Bégué, D., Gohaud, N., Pouchan, C., Cassam-Chenaï, P., & Liévin, J. (2007). A comparison of two methods for selecting vibrational configuration interaction spaces on a heptatomic system: ethylene oxide. *The Journal of chemical physics*, *127*(16), 164115. <https://doi.org/10.1063/1.2795711>
- Bernstein, L.S. & Lynch, D.K. (2009). Small carbonaceous molecules, ethylene oxide (c-C₂H₄O) and cyclopropenylidene (c-C₃H₂): sources of the unidentified infrared bands? *The Astrophysical Journal*, *704*, 226-239. <https://doi.org/10.1088/0004-637X/704/1/226>
- Bertie, J.E. & Jacobs, S.M. (1978). Far infrared and Raman spectra, powder x-ray diffraction, and symmetry of crystalline ethylene oxide. *The Journal of Chemical Physics*, *68*, 97-102. <https://doi.org/10.1063/1.435477>
- Bertie, J.E. & Othen, D.A. (2011). On the Assignment of the Infrared Spectrum of Ethylene Oxide. *Canadian Journal of Chemistry*, *51*(8), 1155-1158. <https://doi.org/10.1139/v73-173>

- Besler, Jr, B.H., Merz, K.M., & Kollman, P.A. (1990). Atomic charges derived from semiempirical methods. *Journal of Computational Chemistry*, 11, 431–439. <https://doi.org/10.1002/jcc.540110404>
- Bichara, L.C., Lanús, H.E., Ferrer, E.G., Gramajo, M.B., & Brandán, S.A. (2011). Vibrational Study and Force Field of the Citric Acid Dimer Based on the SQM Methodology. *Advances in Physical Chemistry*, 2011, 1-10. <https://doi.org/10.1155/2011/347072>
- Biegler-Konig, F., Schonbohm, J. & Bayles, D. (2001). AIM2000 —A Program to Analyze and Visualize Atoms in Molecules. *Journal of Computational Chemistry*, 22(5), 545-559. [https://doi.org/10.1002/1096-987X\(20010415\)22:5<545::AID-JCC1027>3.0.CO;2-Y](https://doi.org/10.1002/1096-987X(20010415)22:5<545::AID-JCC1027>3.0.CO;2-Y)
- Boys, S.F. & Bernardi, F. (1970) The Calculation of Small Molecular Interactions by the Differences of Separate Total Energies. Some Procedures with Reduced Errors. *Molecular Physics*, 19, 553-566. <https://doi.org/10.1080/00268977000101561>
- Brandán, S.A. (2021). Normal internal coordinates Force fields and vibrational study of Species Derived from Antiviral adamantadine, *International Journal of Quantum Chemistry*, 121(2), e26425. <https://doi.org/10.1002/qua.26425>
- Brandán, S.A., López F.M., Montejo, M., González, J.J.L. & Altabef, A.B. (2010). Theoretical and Experimental Vibrational Spectrum Study of 4-Hydroxybenzoic Acid as Monomer and Dimer. *Spectrochimica Acta Part A: Molecular and Biomolecular Spectroscopy*, 75(5), 1422-1434. <https://doi.org/10.1016/j.saa.2010.01.012>
- Cant, N. W., & Armstead, W. J. (1975). Vibrational assignments and force-field calculations for ethylene oxide. *Spectrochimica Acta*, 31(7), 839-853. [https://doi.org/10.1016/0584-8539\(75\)80145-0](https://doi.org/10.1016/0584-8539(75)80145-0)
- Chai, J.-D., & Head-Gordon, M. (2008). Long-Range Corrected Hybrid Density Functionals with Damped Atom-Atom Dispersion Corrections. United States. *Physical Chemistry Chemical Physics*, 10, 6615-6620. <https://doi.org/10.1039/b810189b>
- Daniel, M.F., Desbat, B. & Lassegues, J.C. (1988). Infrared and Raman spectroscopies of rf sputtered tungsten oxide films. *Solid State Ionics*, 28–30, 632-636, 198). [https://doi.org/10.1016/0022-4596\(88\)90062-X](https://doi.org/10.1016/0022-4596(88)90062-X)
- Fogarasi, G., Zhou, X., Taylor, P., & Pulay, P. (1992). The calculation of ab initio molecular geometries: efficient optimization by natural internal coordinates and empirical correction by offset forces. *Journal of the American Chemical Society*, 114, 8191-8201. <https://doi.org/10.1021/ja00047a032>
- Frimand, K., & Jalkanen, K.J. (2002). SCC-TB, DFT/B3LYP, MP2, AM1, PM3 and RHF study of ethylene oxide and propylene oxide structures, VA and VCD spectra. *Chemical Physics*, 279(2-3), 161-178. [https://doi.org/10.1016/S0301-0104\(02\)00457-3](https://doi.org/10.1016/S0301-0104(02)00457-3)
- Frisch, M.J., Trucks, G.W., Schlegel, H.B., Scuseria, G.E., Robb, M.A., Cheeseman, G.R. ... & Fox, D.J. (2009). *Gaussian 09, Revision A.02*. Wallingford CT: Gaussian, Inc.
- Glendening, E.D., Badenhoop, J.K., Reed, A.D., Carpenter, J.E. & Weinhold, F. (1996). *NBO 3.1*. Theoretical Chemistry Institute, University of Wisconsin. Madison, WI.
- Grabowsky, S., Weber, M., Buschmann, J., & Luger, P. (2008). Experimental electron density study of ethylene oxide at 100 K. *Acta crystallographica. Section B, Structural science*, 64(Pt 3), 397–400. <https://doi.org/10.1107/S0108768108010197>
- Hair, S.R., Beswick, J.A. & Janda, K.C. (1988). A quantum mechanical treatment of vibrational mixing in ethylene dimer and rare gas–ethylene complexes. *Journal of Chemical Physics*, 89, 3970–3982. <https://doi.org/10.1063/1.454830>
- Iramain, M.A., Ruiz Hidalgo, J., Sundius, T. & Brandán, S.A. (2022). A Combined Study on Structures and Vibrational Spectra of Antiviral Rimantadine using SQMFF and DFT

- calculations. *Helvion*, 8, e10102. <https://doi.org/10.1016/j.helivon.2022.e10102>
- Issaoui, N., Ghalla, H., Brandán, S. A., Bardak, F., Flakus, H. T., Atac, A., & Oujia, B. (2017). Experimental FTIR and FT-Raman and theoretical studies on the molecular structures of monomer and dimer of 3-thiopheneacrylic acid [Journal Article]. *Journal of Molecular Structure*, 1135, 209–221. <https://doi.org/10.1016/j.molstruc.2017.01.074>
- Lee, C., Yang, W., & Parr, R. G. (1988). Development of the Colle-Salvetti correlation-energy formula into a functional of the electron density. *Physical review. B, Condensed matter*, 37(2), 785–789. <https://doi.org/10.1103/physrevb.37.785>
- Lowe, M.A., Alper, J.S., Kawiecki, R., & Stephens, P.J. (1986). Scaled ab initio force fields for ethylene oxide and propylene oxide. *The Journal of Chemical Physics*, 90(1), 41–50. <https://doi.org/10.1021/j100273a011>
- Mills, I. (1965). Coriolis interactions, intensity perturbations and potential functions in polyatomic molecules. *Pure and Applied Chemistry*, 11(3-4), 325-344. <https://doi.org/10.1351/pac196511030325>
- Mortada, S., Brandán, S.A., Karrouchi, K., El-guourrami, O., Doudach, L., El Bacha, R., Ansar, M., & El Abbes Faouzi, M. (2022). Synthesis, spectroscopic and DFT studies of 5-methyl-1H-pyrazole-3-carbohydrazide N-glycoside as potential anti-diabetic and antioxidant agent. *Journal of Molecular Structure*, 1267, 133652. <https://doi.org/10.1016/j.molstruc.2022.134582>
- Nielsen, A.B., Holder, A.J. (2008). *Gauss View 5.0, User's reference*. Pittsburgh, PA: GAUSSIAN Inc.
- NIST. (n.a.) NIST Chemistry WebBook. NIST Standard Reference Database Number 69. Retrieved from <http://webbook.nist.gov/chemistry>
- Oparaji, O., Zuo, X. & Hallinan Jr., D.T. (2016). Crystallite dissolution in PEO-based polymers induced by water sorption. *Polymer*, 100, 206-218. <https://doi.org/10.1016/j.polymer.2016.08.026>
- Polomska, M., Wolak, J., Hilczer, B. & Szczepanska, L. (1999). NIR–Raman studies of poly(ethylene oxide)+(NH₄)₄H₂(SeO₄)₃ polymer electrolyte. *Solid State Ionics*, 118, 261-264. [https://doi.org/10.1016/S0167-2738\(98\)00458-5](https://doi.org/10.1016/S0167-2738(98)00458-5)
- Pulay, P., Fogarasi, G., Pongor, G., Boggs, J.E. & Vargha, A. (1983). Combination of theoretical ab initio and experimental information to obtain reliable harmonic force constants. Scaled quantum mechanical (QM) force fields for glyoxal, acrolein, butadiene, formaldehyde, and ethylene. *Journal of the American Chemical Society*, 105, 7073. <https://doi.org/10.1021/ja00362a005>
- Rauhut, G. & Pulay, P. (1995). Transferable scaling factors for density functional derived vibrational force fields. *Journal of Physical Chemistry*, 99, 3093–3099. <https://doi.org/10.1021/j100010a019>
- Scheuermann, C., Elizabeth, M.V., Iramain, M.O., Davies, L.E., Manzur, M.E., & Brandan, S.A. (2018). Evaluation of the structural properties of powerful pesticide dieldrin in different media and their complete vibrational assignment. *Elsevier Science; Journal of Molecular Structure*, 1154(2), 392-405. <https://doi.org/10.1016/j.molstruc.2017.10.065>
- Shimanouchi, T. (1972). Tables of Molecular Vibrational Frequencies. *NSRDS*, 39, 1-164.
- Sundius, T. (2002) Scaling of Ab Initio Force Fields by MOLVIB. *Vibrational Spectroscopy*, 29, 89-95. [http://dx.doi.org/10.1016/S0924-2031\(01\)00189-8](http://dx.doi.org/10.1016/S0924-2031(01)00189-8)
- Sundius, T., & Brandán, S. A. (2023). Structural, harmonic force field and vibrational studies of cholinesterase inhibitor tacrine used for treatment of Alzheimer's disease. *Helvion*, 9(6), e17280. <https://doi.org/10.1016/j.helivon.2023.e17280>
- Weiyu, C., Tashiro, K., Hanesaka, M., Takeda, S., Masunaga, H., Sasaki, S., Takata, M. (2009). First detection of lamella-gyroid-cylinder phase

transition of neat polyethylene-poly(ethylene oxide) diblock copolymers on the basis of synchrotron WAXD/SAXS and infrared/Raman spectral measurements. *Journal of Physics: Conference Series*, 184, 012003. <https://doi.org/10.1088/1742-6596/184/1/012003>

Winkler, D.A., Michalewicz, M.T., Wang, F. & Brunger, M.J. (1999). An electron momentum spectroscopy and density functional theory investigation into the complete valence electronic structure of ethylene oxide. *Journal of Physics B: Atomic, Molecular and Optical Physics*, 32, 3239–3253. <https://doi.org/10.1088/0953-4075/32/13/313>

Zhang, H. & Wang, J. (2009). Vibrational spectroscopic study of ionic association in

poly(ethylene oxide)-NH₄SCN polymer electrolytes. *Spectrochimica Acta Part A: Molecular and Biomolecular Spectroscopy*, 71(5), 1927-1931. <https://doi.org/10.1016/j.saa.2008.07.018>

Zhang, H., & Wang, J. (2009). Vibrational spectroscopic study of ionic association in poly(ethylene oxide)-NH₄SCN polymer electrolytes. *Spectrochimica acta. Part A, Molecular and biomolecular spectroscopy*, 71(5), 1927–1931. <https://doi.org/10.1016/j.saa.2008.07.018>

Zhang, H., Wang, J., Xuan, X., & Zhuo, K. (2006). FT-IR studies on interactions of AlCl₃ with PEO–NaSCN polymer electrolytes. *Electrochim. Acta*, 51, 3244-3248. <https://doi.org/10.1016/j.electacta.2005.09.016>